

BATTERIES & SUPERCAPS

Accepted Article

Title: Additive-free hybrid anode of Nb₂O₅-TiO₂ towards low-cost and safe lithium-ion batteries: a green electrode material produced by an environmentally friendly process

Authors: Md Mokhlesur Rahman, Mengqi Zhou, Irin Sultana, Srikanth Mateti, Alexey Falin, Lu Hua Li, Zhong-Shuai Wu, and Ying Chen

This manuscript has been accepted after peer review and appears as an Accepted Article online prior to editing, proofing, and formal publication of the final Version of Record (VoR). This work is currently citable by using the Digital Object Identifier (DOI) given below. The VoR will be published online in Early View as soon as possible and may be different to this Accepted Article as a result of editing. Readers should obtain the VoR from the journal website shown below when it is published to ensure accuracy of information. The authors are responsible for the content of this Accepted Article.

To be cited as: *Batteries & Supercaps* 10.1002/batt.201800092

Link to VoR: <http://dx.doi.org/10.1002/batt.201800092>

The journal for
ELECTROCHEMICAL
ENERGY STORAGE

A Journal of



WILEY-VCH

www.batteries-supercaps.org

ARTICLE

Additive-free hybrid anode of Nb₂O₅-TiO₂ towards low-cost and safe lithium-ion batteries: a green electrode material produced by an environmentally friendly process

Md Mokhlesur Rahman,^{*[a]} Mengqi Zhou,^[a] Irin Sultana,^[a] Srikanth Mateti,^[a] Alexey Falin,^[a] Lu Hua Li,^[a] Zhong-Shuai Wu,^[b] and Ying Chen ^{*[a]}

Abstract: Development of additive-free electrodes with low cost and in an environmentally friendly way represents a sustainable and ecologically friendly energy expansion. Most conventional electrode preparation process is currently facing serious problems due to the addition of various additives/chemicals, particularly binder, carbon black, and toxic *N*-Methyl-2-pyrrolidone, which increase environmental hazard, production cost, and decrease the energy and power density of the battery. A hybrid electrode of Nb₂O₅-TiO₂ for lithium-ion batteries is fabricated for the first time by adopting advanced radio frequency sputtering technique, which requires no supplementary support from additives/chemicals. The Nb₂O₅-TiO₂ electrode reveals high capacity (gravimetric: 214 mAh g⁻¹ at 50 mA g⁻¹; areal: 0.0214 mAh cm⁻² at 5 μA cm⁻²; volumetric: 1,813 mAh cm⁻³ at 5 μA cm⁻²), long-term cyclic stability (gravimetric: 174 mAh g⁻¹ at 0.4 A g⁻¹; areal: 0.0174 mAh cm⁻² at 40 μA cm⁻²; volumetric: 1,474 mAh cm⁻³ at 40 μA cm⁻² after 1000 cycles) and superior rate capability (gravimetric: 115 mAh g⁻¹ at 6.0 A g⁻¹; areal: 0.0115 mAh cm⁻² at 6 mA cm⁻²; volumetric: 974 mAh cm⁻³ at 6 mA cm⁻²), which are better than other reported systems. Such a green chemistry strategy of fabricating additive-free electrode opens up a new way to develop robust energy storage technologies.

Introduction

Lithium-ion batteries (LIBs) are considered as the leading candidates for hybrid, plug-in hybrid, and all electrical vehicles, and possibly for utility applications as well. Considering the progress in large-scale applications, the next generation of LIBs is selected on the basis of their safety/environmental friendliness, cost and energy capacity, which largely depends on the electrode materials used.^[1-3] Currently, commercial anodes are made of graphite that still suffers from potential safety issues (thermal runaway), with the formation of lithium dendrites and a solid-electrolyte interphase (SEI) layer, owing to its low lithiation potential (0.2V vs Li/Li⁺), especially when the LIBs are operated at high current rates.^[4-7] Therefore, to address all of these issues, an alternative anode needs to be developed. Being inherently safe and chemically compatible with the electrolyte, low voltage insertion for Li⁺ and fast Li⁺ insertion/removal host as well as low environmental impact and cost,^[8,9] titanium-oxide-based materials,

including both Li-titanates and various TiO₂ polymorphs, are considered to be alternatives to carbonaceous anodes in LIBs. The rutile phase of TiO₂ is the most common natural form, as it is the most thermodynamically stable phase under standard conditions and capable to provide high capacity and better lithium electrochemical activity in its nanostructured form.^[10, 11] However, nanostructured TiO₂ is prone to suffer from severe aggregation, which dramatically diminishes its rate capability and cyclability.^[12] In addition to rutile TiO₂, niobium pentoxide (Nb₂O₅) is also an ideal high power electrode material in LIBs, as it is relatively inexpensive, environmentally benign, stable in a wide range of temperature and pH conditions, and most importantly improved cell safety due to a higher discharge cut-off voltage (≥ 1.0V vs Li/Li⁺) which reduces dangerous high-temperature reactions.^[13-16] However, its intrinsic poor electronic conductivity and capacity decay resulted from pulverization during charge-discharge process limit its practical application in LIBs. Also, it is still challenging to develop efficient but simple ways to enhance the utilization of electroactive Nb₂O₅.^[13, 17-20]

To circumvent these problems with TiO₂ and Nb₂O₅, the hybridization concept can potentially be used. It has been demonstrated that hybrid oxide systems exhibit some new properties and superior to single-phase oxides, the hybrid systems integrate several types of functional materials that can synergistically enhance the intrinsic properties of each component such as electrical/ionic conductivity, electrochemical reactivity, and mechanical stability.^[21-25] The underlying problem with the conventional procedure for the preparation of battery electrodes is time consuming involving unhealthy multiple steps, including materials synthesis with toxic reagents, slurry formation, coating onto current collectors, and drying in vacuum. Furthermore, carbon black, polymeric binders and organic solvent (*N*-Methyl-2-pyrrolidone) are commonly included during slurry preparation for electrical conduction and better physical contacts between particles and current collector, respectively.^[26-30] Basically, addition of various additives to the electrodes generates 3 major problems:^[31, 32] i) an extra weight (10-40%, depending on the electrode materials used) of the electrode is increased; ii) inhomogeneous blend of carbon black, binders, and nanoparticles (active materials) makes the diffusion paths of the ions and electrons unclear, leading to model and characterization difficulties; and iii) complicated procedure and various additives lead to environmental hazard as well as high cost of the electrodes.

Previously, nanomaterials in the form of nanowires and nanotubes with no binder and carbon have been developed and investigated as electrodes for energy storage.^[33-37] However, fully additive-free electrode films in the form of nanoparticles are hardly reported. More specifically, the hybridization of both nanoparticles of TiO₂ and Nb₂O₅ as an additive-free electrode has not yet been established. In 2016, hybridization of Nb-doped TiO₂ and Nb₂O₅

[a] Dr. M.M. Rahman, Dr. M. Zhou, Dr. I. Sultana, Dr. S. Mateti, Dr. A. Falin, Dr. L. H. Li, Prof. Y. Chen
Institute for Frontier Materials, Deakin University, Geelong Waurn Ponds, VIC 3216 (Australia)
E-mail: m.rahman@deakin.edu.au; ian.chen@deakin.edu.au

[b] Prof. Z. S. Wu
Dalian National Laboratory For Clean Energy, Dalian Institute of Chemical Physics, Chinese Academy of Sciences, 457 Zhongshan Road, Dalian 116023, China

Supporting information for this article is given via a link at the end of the document.

ARTICLE

was studied by Yu et al. [38] In that study, they fabricated core-shell heterostructures where Nb-doped TiO₂ rod used as a core and Nb₂O₅ nanosheet as a shell. Recently, Liu et al. [12] have also demonstrated a heterogeneous composite of TiO₂-Nb₂O₅. In this composite, nanoparticles of TiO₂ were surrounded on the nanosheets of Nb₂O₅. However, the above-mentioned hybridized systems cannot be claimed as additive-free systems as they used binder and carbon black for the preparation of electrode. Moreover, various reagents were used in their synthesis process. Despite the tremendous research efforts devoted to investigating a wide variety of hybrid materials for electrochemical performances in recent years, however, the hybrid systems are still limited to high crystalline ones incorporated with high level of binder and carbon additives. [39-41] Hence, it would be advantageous but quite challenging to develop a simplistic method of fabrication binary electrode system, particularly metal oxide without using any additives/chemicals but with superior electrochemical performances.

Herein, we for the first time report additive free Nb₂O₅-TiO₂ electrode deposited on Cu foil fabricated by hybridization of both nanoparticles of TiO₂ and Nb₂O₅ *via* ultrafast sputtering technique by combining titanium (Ti) and niobium (Nb) target together at the same time. Most importantly, no reagents were used in this synthesis process. The obtained hybridized Nb₂O₅-TiO₂ electrode was used directly without further incorporation of any carbon, binder or organic solvent. A single oxide electrode of Nb₂O₅ and TiO₂ was also fabricated for comparison, using same technique. A series of electrodes with different deposition times of 0.5, 1.0, and 2.0 h was fabricated and electrodes were identified as Nb₂O₅-TiO₂ (0.5h), Nb₂O₅-TiO₂ (1h), Nb₂O₅-TiO₂ (2h), Nb₂O₅ (1h), and TiO₂ (1h), respectively. The electrode was operated within the safe potential window of 1.0-3.0V (vs Li/Li⁺) and hybrid Nb₂O₅-TiO₂ (1h) electrode with special pearls-chain like morphology delivers a promising reversible capacity of gravimetric 214 mAh g⁻¹ at 50 mA g⁻¹; areal 0.0214 mAh cm⁻² at 5 μA cm⁻² and volumetric 1,813 mAh cm⁻³ at 5 μA cm⁻² after 500 cycles. The electrode exhibits superior long-term cyclic stability with a retained capacity of gravimetric 174 mAh g⁻¹ at 0.4 A g⁻¹; areal 0.0174 mAh cm⁻² at 40 μA cm⁻² and volumetric 1,474 mAh cm⁻³ at 40 μA cm⁻² even after 1000 cycles. The rate capability of the Nb₂O₅-TiO₂ (1h) is quite high and a reversible capacity of gravimetric 115 mAh g⁻¹ at 6.0 A g⁻¹; areal 0.0115 mAh cm⁻² at 6 mA cm⁻² and volumetric 974 mAh cm⁻³ at 6 mA cm⁻² is achieved. These results demonstrate that additive-free Nb₂O₅-TiO₂ materials have great potential to be used as safe electrode for LIBs. Moreover, such a special electrode architecture can be used in Li-ion micro-batteries, as it demands high energy and high power on a small footprint area.

Results and Discussion

Figure 1a compares the XRD patterns of the hybrid Nb₂O₅-TiO₂ (0.5h), Nb₂O₅-TiO₂ (1h), and Nb₂O₅-TiO₂ (2h) electrodes. All XRD patterns consist of mixed metal oxide phases of Nb₂O₅ and TiO₂, respectively. Diffraction peaks for the Nb₂O₅ are indexed to the orthorhombic crystal structure (JCPDS Card No. 00-030-0873) and peaks are located at around 28.5, 36.7, 45.0, 46.1, 55.0, and 71.2°, which are assigned to the (180), (181), (2110),

(002), (182), and (382) reflections, respectively. In the case of TiO₂, all diffraction peaks are well indexed to the rutile TiO₂ phase (JCPDS Card No. 00-004-0551) with tetragonal crystal system. The diffraction peaks for rutile TiO₂ are located at 27.4, 39.1, 41.2, 54.3, 56.6, 64.0, and 68.9°, corresponding to the (110), (200), (111), (211), (220), (310), and (301) reflections, respectively. It is visualised that Nb₂O₅-TiO₂ (2h) electrode shows strong diffraction peaks, which may be due to longer deposition time. No other peaks for anatase or brookite were detected in the electrode, signifying Nb₂O₅-TiO₂ electrode composes of only rutile TiO₂ and orthorhombic Nb₂O₅. To further confirm the composition of Nb₂O₅-TiO₂ electrode, X-ray photoelectron spectroscopy (XPS) was carried out (Figure 1b-d). Species of Nb, Ti, O, and C are detected as elements in the Nb₂O₅-TiO₂ electrode, suggesting high purity of the sample (Figure 1b). High-resolution XPS spectra for the Nb3d region shows two peaks at around 207.9 eV for Nb3d_{5/2} and 210.5 eV for Nb3d_{3/2} regions (Figure 1c), in good agreement with the binding energies of Nb₂O₅, [16, 42] confirming the presence of Nb₂O₅ in the Nb₂O₅-TiO₂ electrode. Similarly, two peaks of Ti2p are centred at 459 and 465 eV for the regions of Ti2p_{3/2} and Ti2p_{1/2}, respectively (Figure 1d), indicative of the existence of TiO₂ in the hybrid electrode. [43, 44]

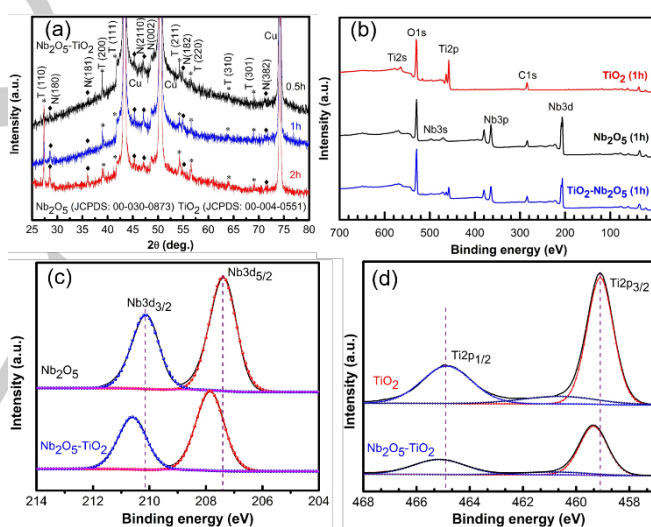


Figure 1. a) XRD patterns of the Nb₂O₅-TiO₂ (0.5 h), Nb₂O₅-TiO₂ (1 h), and Nb₂O₅-TiO₂ (2 h) electrodes. b) wide survey scan of XPS of the Nb₂O₅-TiO₂ (1h) Nb₂O₅ (1h) and TiO₂ (1h) electrodes. c) high-resolution XPS spectra of Nb3d region. d) high-resolution XPS spectra of Ti2p region.

Surface morphologies of the Nb₂O₅-TiO₂ electrode films as a function of deposition time were analysed by SEM (Figure 2). It is clearly seen that surface morphologies of the electrode films feature pearls-chain like structure composed of nanoparticles. The formation of pearls-chain is not obvious when the deposition time is shorter (0.5 h) (Figure 2a, b) and longer (2 h) (Figure 2e, f) as well. The formation of pearls-chain became more significant with the deposition time of 1 h (Figure 2 c, d). The films deposited over 2 h, however, exhibits much coarser particles than that of 1 h and 0.5 h deposited films, losing pearls-chain like morphology (Figure 2e,f). As a result, such a special pearls-chain morphology

ARTICLE

of the $\text{Nb}_2\text{O}_5\text{-TiO}_2$ (1h) electrode may enhance Li^+ ions storage properties. Figure 2g shows the image of the cross-section of $\text{Nb}_2\text{O}_5\text{-TiO}_2$ (1h) electrode film. A layer of about 123.2 nm thick is measured between the platinum layer and the copper layer. However, a gold layer of about 5 nm thick (probably too thin to discern) is expected, since we gold-coated the specimen for conductivity before putting it in the FIB-SEM. Therefore, we assume that the rest of the 118 nm layer may be due to the $\text{Nb}_2\text{O}_5\text{-TiO}_2$ materials. SEM images of Cu foil substrate, Nb_2O_5 (1 h) and TiO_2 (1 h) electrodes are presented in Figure S1.

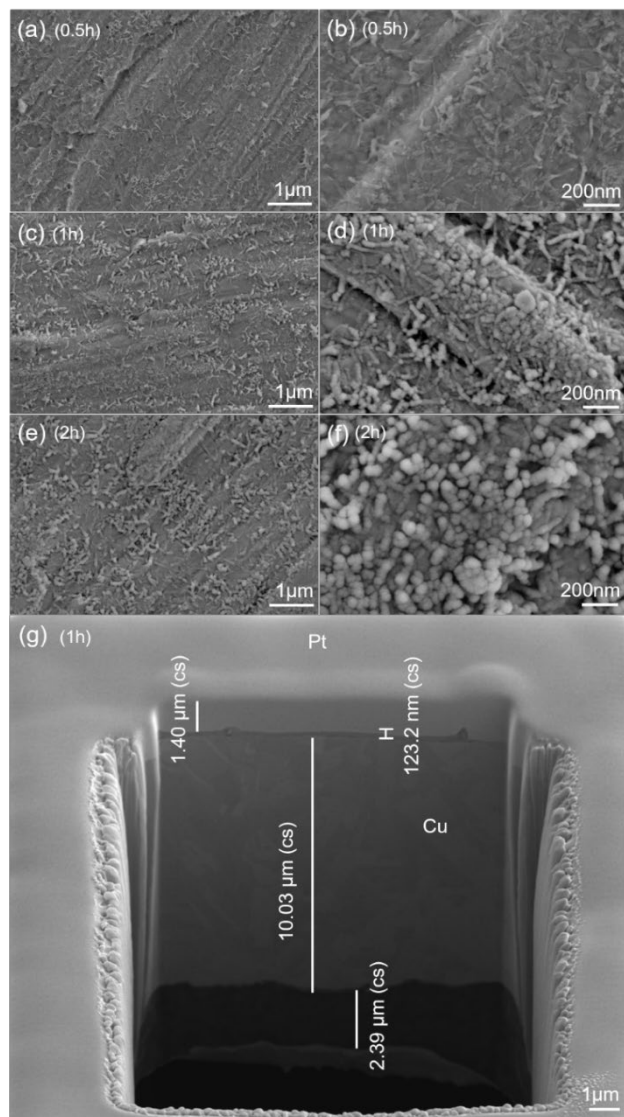


Figure 2. SEM images of the electrodes: a, b) $\text{Nb}_2\text{O}_5\text{-TiO}_2$ (0.5 h), c, d) $\text{Nb}_2\text{O}_5\text{-TiO}_2$ (1 h), e, f) $\text{Nb}_2\text{O}_5\text{-TiO}_2$ (2 h); and g) cross-section image of the $\text{Nb}_2\text{O}_5\text{-TiO}_2$ (1h) electrode.

The morphological and physical structure of the electrodes were further evaluated using AFM technique. Figure 3a-c present AFM topography images with an area of $0.25 \mu\text{m}^2$ ($0.5 \mu\text{m} \times 0.5 \mu\text{m}$) obtained on the $\text{Nb}_2\text{O}_5\text{-TiO}_2$ electrodes. Clearly, no significant

difference is observed between $\text{Nb}_2\text{O}_5\text{-TiO}_2$ (0.5h) and $\text{Nb}_2\text{O}_5\text{-TiO}_2$ (2h) electrodes, however, pearls-chain like morphology is visualised in the image of $\text{Nb}_2\text{O}_5\text{-TiO}_2$ (1 h) electrode. More AFM images of the electrodes can be found in Figure S2. An area of $0.25 \mu\text{m}^2$ for each electrode was selected for the calculation of particles sizes as shown in Figure 3d. An approximate particle sizes were measured to be $34 \pm 17 \text{ nm}$ for $\text{Nb}_2\text{O}_5\text{-TiO}_2$ (0.5 h), $28 \pm 11 \text{ nm}$ for $\text{Nb}_2\text{O}_5\text{-TiO}_2$ (1h), and $35 \pm 12 \text{ nm}$ for $\text{Nb}_2\text{O}_5\text{-TiO}_2$ (2 h) electrodes, respectively. Within the same area of $0.25 \mu\text{m}^2$, the measured average particle sizes were $34 \pm 19 \text{ nm}$ for Nb_2O_5 (1h) and $40 \pm 20 \text{ nm}$ for TiO_2 (1h) electrodes, respectively (Figure S3). AFM topography images and corresponding particles size analysis reveal that $\text{Nb}_2\text{O}_5\text{-TiO}_2$ (1h) electrode shows smaller particles size than that of the other electrodes.

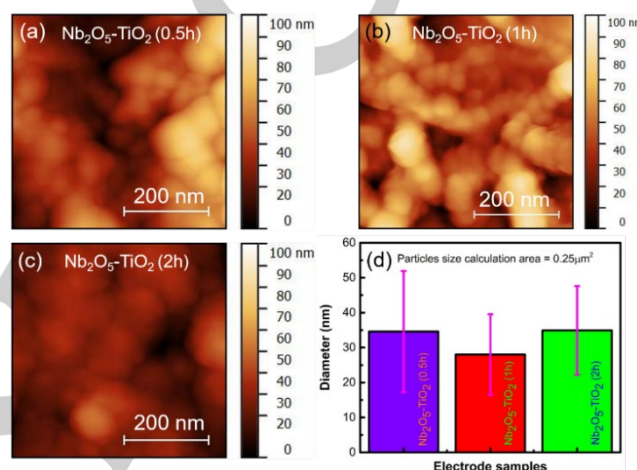


Figure 3. AFM topography images and average particle sizes of the electrodes: a-c) topography of a) $\text{Nb}_2\text{O}_5\text{-TiO}_2$ (0.5 h), b) $\text{Nb}_2\text{O}_5\text{-TiO}_2$ (1 h), c) $\text{Nb}_2\text{O}_5\text{-TiO}_2$ (2h) electrodes. d) average particle sizes measured within the area of $0.25 \mu\text{m}^2$ from (a-c).

To achieve more structural information of the electrodes, AFM data was used to evaluate the particles size distribution. Figure 4 a, c, e demonstrate AFM mages of the electrodes and their corresponding particles size distribution results are depicted in Figure 4b, d, f. As revealed in Figure 4b, d, f, particles size between 0-100 nm for $\text{Nb}_2\text{O}_5\text{-TiO}_2$ (0.5 h), 10-70 nm for $\text{Nb}_2\text{O}_5\text{-TiO}_2$ (1h), and 10-90 nm for $\text{Nb}_2\text{O}_5\text{-TiO}_2$ (2h) electrodes are spotted. No particles size over 70 nm is realised in the $\text{Nb}_2\text{O}_5\text{-TiO}_2$ (1h) electrode. Overall, high percentage distribution of smaller particles is observed in the $\text{Nb}_2\text{O}_5\text{-TiO}_2$ (1h) electrode. We further conducted roughness evaluation of the electrodes in 3 different areas of $900 \mu\text{m}^2$, $1.0 \mu\text{m}^2$, and $0.25 \mu\text{m}^2$, respectively. Figure 5a-c shows AFM topography within the area of $900 \mu\text{m}^2$ ($30 \mu\text{m} \times 30 \mu\text{m}$) and the measured corresponding surface area roughness is demonstrated in Figure 5d. Roughness of the $\text{Nb}_2\text{O}_5\text{-TiO}_2$ (1h) electrode film measured in 3 three different areas is higher than other two electrodes of $\text{Nb}_2\text{O}_5\text{-TiO}_2$ (0.5h) and $\text{Nb}_2\text{O}_5\text{-TiO}_2$ (2 h) (Figure 5d, e, f), respectively, implying that higher surface area roughness of the $\text{Nb}_2\text{O}_5\text{-TiO}_2$ (1h) electrode may work as an electrolyte reservoir, which could facilitate electrolyte diffusion into the bulk of the electrode. AFM topography within the same area of $900 \mu\text{m}^2$ ($30 \mu\text{m} \times 30 \mu\text{m}$) and

ARTICLE

the measured corresponding roughness for the TiO₂ (1h) and Nb₂O₅ (1h) electrodes can also be found in Figure S4.

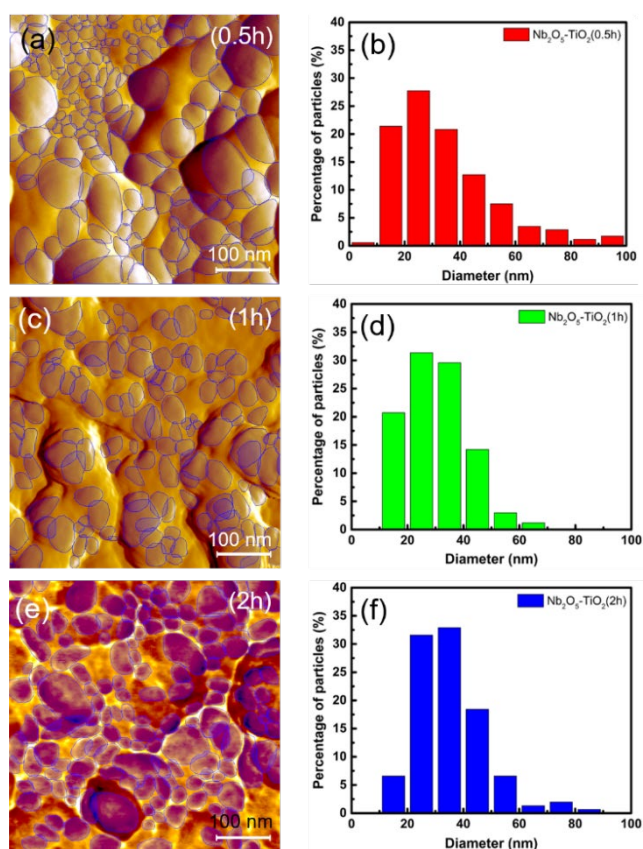


Figure 4. AFM images and corresponding particles size distribution: a, b) Nb₂O₅-TiO₂ (0.5 h), c, d) Nb₂O₅-TiO₂ (1 h), e, f) Nb₂O₅-TiO₂ (2 h) electrodes.

To understand Li⁺ ions intercalation/de-intercalation behaviour of the electrode films, cyclic voltammetry (CV) was carried out within the potential range of 1.0-3.0V (vs Li/Li⁺) at a scan rate of 0.5 mVs⁻¹. Figure 6 compares the CV curves between Nb₂O₅, TiO₂, and Nb₂O₅-TiO₂ electrodes. Electrodes fabricated with 1.0 h deposition time were selected for CV analysis. As shown in Figure 6a for Nb₂O₅ electrode, cathodic peaks at ~1.3V in the 1st cycle and ~1.4V in the subsequent cycles (reduction-Nb⁵⁺/Nb⁴⁺) and anodic peaks at ~2.0 V (oxidation- Nb⁴⁺/Nb⁵⁺) were detected.^[16] A redox peaks of 1.4/2.0V represents intercalation/de-intercalation process of Li⁺ ions into the crystal structure of the Nb₂O₅ electrode according to the equation below:



Figure 6b shows the representative CV curves of the rutile TiO₂. In the cathodic scan, peaks at ~1.6V in the 1st cycle and ~1.5V in the subsequent cycles was observed. A redox peaks (cathodic/anodic) at ~1.5/2.1V was maintained in the subsequent cycles.^[45, 46] The intercalation/de-intercalation process of Li⁺ ions into the crystal structure of the rutile TiO₂ can be summarised as below:

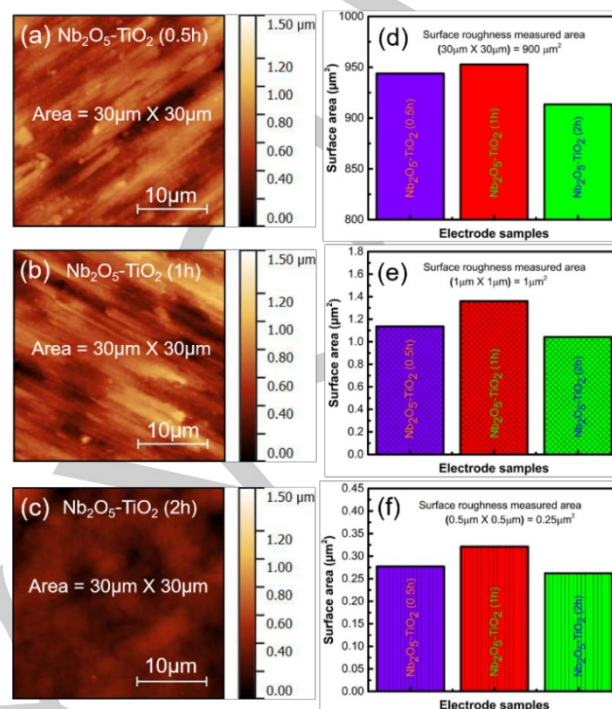


Figure 5. AFM topography and measured approximate values of surface area roughness parameter of the electrodes: a-c) AFM topography with area of 900 μm² (30 μm x 30 μm), d) corresponding surface area roughness values measured from (a-c) for the same area of 900 μm², e, f) surface area roughness values measured from area of (e) 1 μm² (1 μm x 1 μm) and (f) 0.25 μm² (0.5 μm x 0.5 μm), respectively.

In the case of hybridized Nb₂O₅-TiO₂ electrode, however, broad cathodic and anodic peaks are formed (Figure 6c), which could be related to the combination of Nb₂O₅ peak and TiO₂ peak together. A broad cathodic peak located in the range of 1.2-1.8V, corresponds to the potential profiles of the discharge process, involving Li⁺ ions intercalation first in to the crystal structure of TiO₂ followed by Nb₂O₅ in the Nb₂O₅-TiO₂ electrode. Similarly, broad anodic peak located at ~1.7-2.3V is corresponding to the charge process, involving Li⁺ ions de-intercalation from the crystal structure of the Nb₂O₅-TiO₂ electrode. The CV curve of the first and fifth cycles almost overlap, demonstrating good reversibility of the electrochemical reactions in the Nb₂O₅-TiO₂ electrode after the initial cycle.

ARTICLE

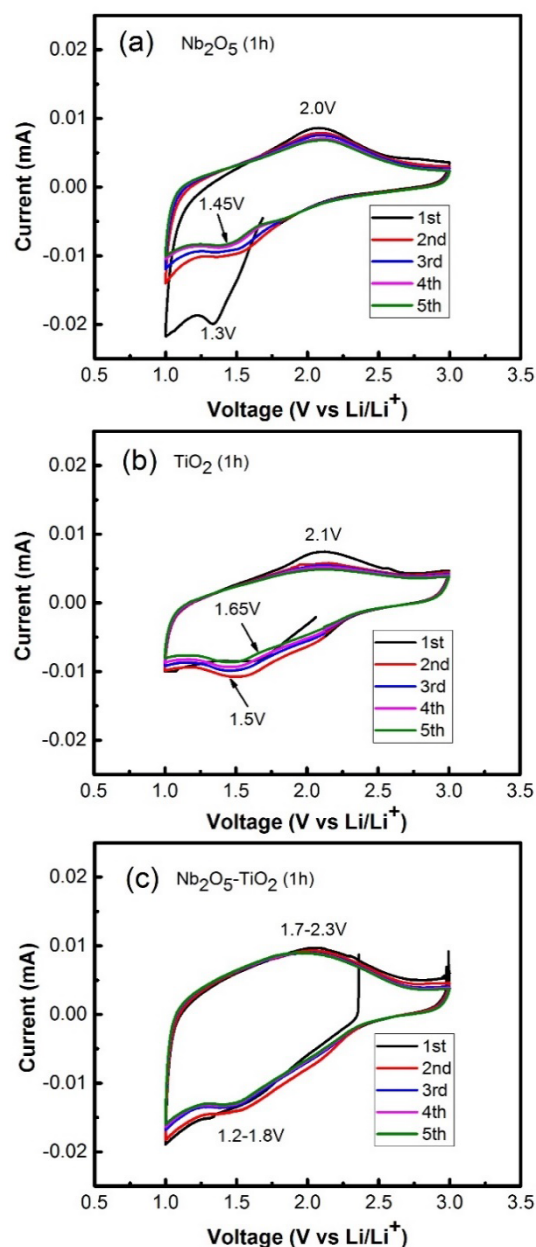


Figure 6. Cyclic voltammograms of the Nb_2O_5 (1h), TiO_2 (1h) and $\text{Nb}_2\text{O}_5\text{-TiO}_2$ (1h) electrodes at a scan rate of 0.5 mVs^{-1} within the potential range of 1.0-3.0V (vs Li/Li^+).

Figure 7a compares electrochemical performance between $\text{Nb}_2\text{O}_5\text{-TiO}_2$ (0.5 h), $\text{Nb}_2\text{O}_5\text{-TiO}_2$ (1h), and $\text{Nb}_2\text{O}_5\text{-TiO}_2$ (2h) electrodes, respectively. The $\text{Nb}_2\text{O}_5\text{-TiO}_2$ (1 h) electrode displays a high reversible capacity of 214 mAh g^{-1} at 50 mA g^{-1} ; areal $0.0214 \text{ mAh cm}^{-2}$ at $5 \mu\text{A cm}^{-2}$ and volumetric $1,813 \text{ mAh cm}^{-3}$ at $5 \mu\text{A cm}^{-2}$ after 500 cycles. Relatively low reversible capacities of 105 mAh g^{-1} for $\text{Nb}_2\text{O}_5\text{-TiO}_2$ (0.5 h) and 163 mAh g^{-1} for $\text{Nb}_2\text{O}_5\text{-TiO}_2$ (2h) electrodes were measured in an identical testing condition. Galvanostatic charge-discharge profiles of the $\text{Nb}_2\text{O}_5\text{-TiO}_2$ (1h) electrode are demonstrated in Figure 7b. Figure 7b shows the 1st and 2nd cycles charge-discharge potential profiles and profile for other selected cycles of 100, 200, 300, 400, and

500th, respectively. It is important to note that $\text{Nb}_2\text{O}_5\text{-TiO}_2$ (1h) electrode displays sloping charge-discharge profiles rather than obvious plateau (results are quite consistent with the CV curves), which could be related to the low crystallinity of the sample.^[47,48] A large capacity of 510 mAh g^{-1} was measured in the first discharge process whereas charge capacity was 372 mAh g^{-1} , even though delivering a commendable Coulombic efficiency of $\sim 73\%$ in the first cycle, however, this irreversible capacity loss could be related to the side reactions of the electrode materials.^[47] High Coulombic efficiency of $\sim 100\%$ was achieved for all electrodes after initial few cycles, indicating very good reversibility of the electrodes (Figure 7a).

The influence of deposition time on the electrochemical performance was further investigated by rate capability test of the electrodes (Figure 7c). The obtained data show that the $\text{Nb}_2\text{O}_5\text{-TiO}_2$ (1h) electrode exhibits superior rate performance over $\text{Nb}_2\text{O}_5\text{-TiO}_2$ (0.5h) and $\text{Nb}_2\text{O}_5\text{-TiO}_2$ (2h) electrodes. The reversible capacities of 261 mAh g^{-1} at 0.1 A g^{-1} ; 211 mAh g^{-1} at 0.2 A g^{-1} ; 176 mAh g^{-1} at 0.3 A g^{-1} ; 159 mAh g^{-1} at 0.6 A g^{-1} ; 137 mAh g^{-1} at 1.5 A g^{-1} ; 126 mAh g^{-1} at 3.0 A g^{-1} ; and 115 mAh g^{-1} at 6.0 A g^{-1} were achieved for the $\text{Nb}_2\text{O}_5\text{-TiO}_2$ (1h) electrode. A capacity recovery of 231 mAh g^{-1} (88.5 % retention) was obtained when electrode was brought back to 0.1 A g^{-1} after 50 cycles whereas it was 133 mAh g^{-1} (82 % retention) for $\text{Nb}_2\text{O}_5\text{-TiO}_2$ (0.5 h) and 182 mAh g^{-1} (80 % retention) for $\text{Nb}_2\text{O}_5\text{-TiO}_2$ (2h) electrodes, respectively. Such an excellent electrochemical performance of the $\text{Nb}_2\text{O}_5\text{-TiO}_2$ (1h) electrode was further investigated as shown in Figure 7d. The electrode is capable to sustain over long-term 1000 cycles with a retained capacity of gravimetric 174 mAh g^{-1} at 0.4 A g^{-1} ; areal $0.0174 \text{ mAh cm}^{-2}$ at $40 \mu\text{A cm}^{-2}$ and volumetric $1,474 \text{ mAh cm}^{-3}$ at $40 \mu\text{A cm}^{-2}$. A high Coulombic efficiency of almost 100 % was maintained over 1000 cycles (Figure 7d).

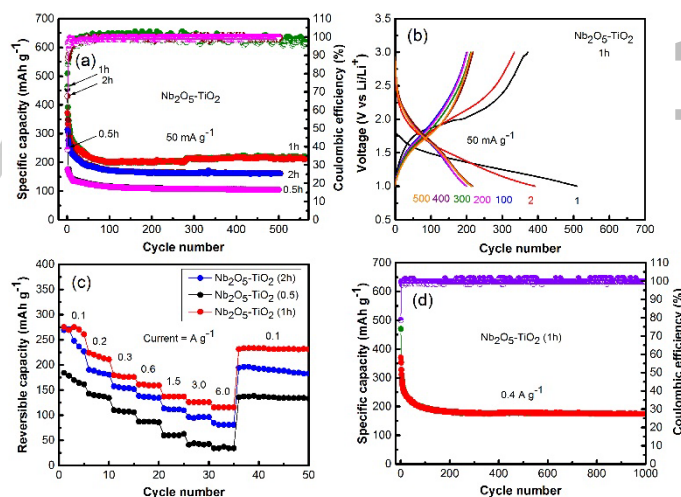


Figure 7. Electrochemical performance of the electrodes: a) cycling performance and corresponding Coulombic efficiencies of the electrodes at a current density of 50 mA g^{-1} . b) corresponding charge-discharge potential profiles obtained at 50 mA g^{-1} for the selected cycles of the $\text{Nb}_2\text{O}_5\text{-TiO}_2$ (1h) electrode. c) rate capability test at different current densities. d) long-term cycling performance and corresponding Coulombic efficiency of the $\text{Nb}_2\text{O}_5\text{-TiO}_2$ (1h) electrode at a current density of 0.4 A g^{-1} up to 1000 cycles.

ARTICLE

As the Nb₂O₅-TiO₂ (1h) electrode exhibits better electrochemical performance over Nb₂O₅-TiO₂ (0.5h) and Nb₂O₅-TiO₂ (2h) electrodes, therefore, Nb₂O₅-TiO₂ (1h) electrode was compared to the single-phase electrode of only Nb₂O₅ or TiO₂. For this comparison, Nb₂O₅ and TiO₂ electrode films were fabricated using the same conditions as it does for the Nb₂O₅-TiO₂ (1h) electrode. Figure 8a reveals electrochemical performance between electrodes and shows that Nb₂O₅-TiO₂ (1h) is capable to achieve a discharge capacity of 218 mAh g⁻¹ at 50 mA g⁻¹ after 400 cycles, which is better than that of 177 mAh g⁻¹ for TiO₂ (1h) and 155 mAh g⁻¹ for Nb₂O₅ (1h) electrodes, respectively. The capacity retention of ~43 % (in respect to initial discharge capacity) is also measured for Nb₂O₅-TiO₂ (1h) electrode, higher than Nb₂O₅ (1h) (30 %) and TiO₂ (1h) (34 %). Figure 8a also compares Coulombic efficiencies between electrodes. The initial Coulombic efficiencies of ~73, 67, and 55% were measured for the Nb₂O₅-TiO₂ (1h), TiO₂ (1h), and Nb₂O₅ (1h) electrodes, respectively. Galvanostatic charge-discharge profiles of the Nb₂O₅ (1h) and TiO₂ (1h) electrodes obtained at 50 mA g⁻¹ for the selected cycles of 1st, 2nd, 100th, 200th, 300th, and 400th are shown in Figure 8b, c. However, capacities of all electrodes decrease sharply for the initial several cycles and stabilise in the extended cycling. During initial intercalation, Li⁺ ions are inserted into the Nb₂O₅-TiO₂ or Nb₂O₅ or TiO₂ electrode thin films. Some of these Li⁺ ions are trapped and cannot fully reverse in the charge process because some of the extra sites in the electrodes are irreversible for Li⁺ ions. [49] It is anticipated that more and more inactive Li⁺ ions are accumulated in the electrode material. This process naturally intensifies the rate of electrolyte decomposition and the subsequent SEI formation for the initial several cycles. [50, 51] This phenomenon may account for the observed capacity loss in the initial several cycles.

An inspiring electrochemical performance of the hybrid Nb₂O₅-TiO₂ electrode is not only better than single-phase electrode of either Nb₂O₅ or TiO₂, but also even better than other reported additive-based Nb₂O₅ and TiO₂ systems, as summarized in Table S1. [12, 16, 19, 38, 52-58] The superior electrochemical performance of the Nb₂O₅-TiO₂ (1h) electrode over Nb₂O₅-TiO₂ (0.5h), Nb₂O₅-TiO₂ (2h), Nb₂O₅ (1h) and TiO₂ (1h) electrodes can be credited to its distinctive electrode architecture and synergistic effects between component as described below:

First, SEM and AFM observations demonstrate that Nb₂O₅-TiO₂ (1h) electrode film features pearls-chain like morphology consisting of numerous nanoparticles, which are attached one after one. Such a unique arrangement is capable to form void due to the interconnection gaps among chains. Once impregnated by the electrolyte, the voids function as an electrolyte reservoir, facilitates electrolyte diffusion into the bulk of the electrode, thus improving Li⁺ ions transport path.

Second, among all electrode films, the Nb₂O₅-TiO₂ (1h) electrode shows small particles size (28 ± 11nm). Smaller particles not only improve ionic conductivity but also minimise extra strain developing in the electrode during repeated cycling process. Hence, Nb₂O₅-TiO₂ (1h) electrode is accomplished to bear repeated expansion and contraction much better than other

electrodes by enabling charge transfer (both ionic and electronic) over shorter distances.

Third, roughness of the electrode films is another important factor needs to be considered. Higher roughness is measured for the Nb₂O₅-TiO₂ (1h) electrode film as shown in Figure 5. High surface roughness could hold electrolyte and provide large effective area for most particles contribution to the charge-discharge process. Additionally, during cycling both Nb₂O₅ and TiO₂ nanoparticles act as mutual buffer due to synergistic effect which has an encouraging impact in controlling the volume change effects in the electrode, [12,41] promoting a better electrochemical performance of the Nb₂O₅-TiO₂ electrode over their counter part of Nb₂O₅ or TiO₂.

Fourth, as binder is not used in the Nb₂O₅-TiO₂ (1h) electrode system, therefore grain boundaries and interface charge transfer resistance are likely to be reduced significantly. [59] As a result, high electron transport along the lattices of electroactive Nb₂O₅-TiO₂ is expected. Furthermore, a tight contact between Nb₂O₅-TiO₂ and the surface of conductive Cu foil substrate is also realised which permits for rapid electron collection and transportation to the outer circuit, providing high rate capability of the cell.

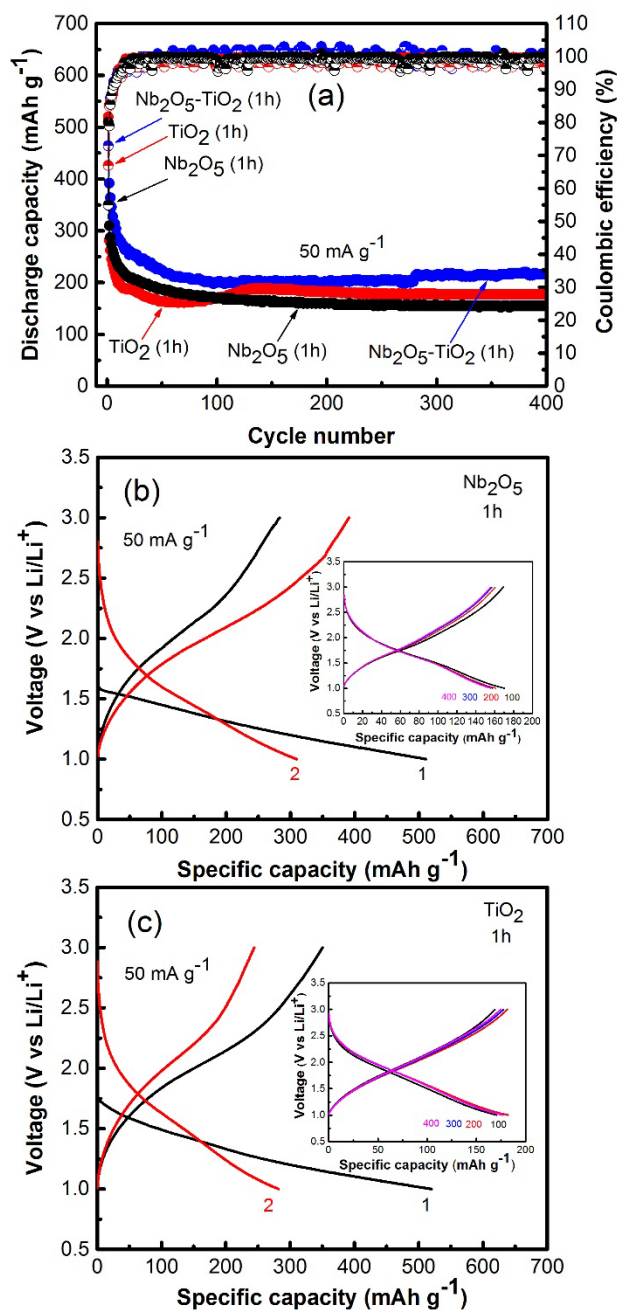


Figure 8. Electrochemical performance of the Nb₂O₅-TiO₂ (1h), Nb₂O₅ (1h), and TiO₂ (1h) electrodes: a) cycling performance and corresponding Coulombic efficiencies at a current density of 50 mA g⁻¹ up to 400 cycles. b,c) corresponding charge-discharge profiles obtained at 50 mA g⁻¹ for the selected cycles (inset shows the curves for the 100th, 200th, 300th, and 400th cycle) of the Nb₂O₅ (1h) and TiO₂ (1h) electrodes, respectively.

Conclusions

In summary, we have developed one-step sputtering technique to achieve an additive-free hybrid electrode of Nb₂O₅-TiO₂ by combining titanium (Ti) and niobium (Nb) target together. The process is fast, easy, and environmentally friendly which requires no additional chemicals/reagents. The electrode was used directly after being deposited on the copper (Cu) foil. The hybrid Nb₂O₅-TiO₂ electrode with 1h deposition time demonstrates superior electrochemical performance over single-phase electrode of either Nb₂O₅ or TiO₂ film. Furthermore, the hybrid Nb₂O₅-TiO₂ electrode is also dominating electrochemical performance over other reported additive-based Nb₂O₅-TiO₂ or Nb₂O₅ or TiO₂ systems. The superior electrochemical performance of the Nb₂O₅-TiO₂ electrode could be accredited to its pearls-chain like architecture, small particles size, high surface roughness, and synergistic coupling effects from individual component. Our electrode fabrication strategy can potentially be used to fabricate a wide range of additive free electrodes (anode and cathode) for advanced energy storage technologies.

Experimental Section

Fabrication of Nb₂O₅-TiO₂ electrode films

The ONYX-2TM Magnetron Sputtering was used for the fabrication of Nb₂O₅-TiO₂ electrode films. During deposition, both Ti and Nb targets were used together where copper (Cu) foil used as substrate. The Cu foil substrate was placed on the sample holder and then the holder was inserted inside the chamber. The process was carried out under vacuum with a sputtering gas flow, a mixture of pure argon/oxygen (Ar/O₂) of 30/15 sccm. A radio frequency power of 250 W was applied to the targets. Three different deposition times of 0.5, 1.0, and 2.0 h was selected. For comparison, an identical condition was used to fabricate Nb₂O₅ and TiO₂ electrode film using only Nb and Ti target, respectively. According to the deposition time, the fabricated electrodes were identified as Nb₂O₅-TiO₂ (0.5h), Nb₂O₅-TiO₂ (1h), Nb₂O₅-TiO₂ (2h), Nb₂O₅ (1h), and TiO₂ (1h), respectively.

Films characterization

X-ray diffraction (XRD) data were collected from the film samples on a PANalytical X'Pert Pro instrument using a CuK α radiation source ($\lambda = 1.54181 \text{ \AA}$) and operated at 40 kV with a 50 mA current. A Kratos AXIS Nova spectrometer (Kratos Analytical Ltd, U.K.) equipped with a monochromated Al K α X-ray source ($h\nu = 1486.6 \text{ eV}$) operating at 150 W used for X-ray photoelectron spectroscopy (XPS) analysis. Morphologies of all film samples were examined using scanning electron microscopy (SEM, Carl Zeiss Supra 55 VP Instrument). Thicknesses of the electrode was measured by FEI Quanta 3D FEG (SEM/FIB) microscope using the Everhart-Thornley detector. An atomic force microscope (AFM, Cypher Asylum Research) was used to analyse topography, particles size and particles size distribution of the electrode films.

Electrochemical characterization

Thin film electrodes of Nb₂O₅-TiO₂, Nb₂O₅, and TiO₂ were used directly for the assembly of CR-2032 coin-type cells where Li foil as the counter/reference electrode and a microporous polypropylene film used as a separator. An electrolyte of 1M LiPF₆ in a mixture of ethylene carbonate (EC) and diethylene carbonate (DEC) with a volume ratio of 1:1 was used. Galvanostatic discharge-charge on the

ARTICLE

cells was performed within the cut-off voltages of 1.0-3.0V (vs Li/Li⁺) at different current densities using a Land Battery Testing System.

Acknowledgements

The work was supported by ARC Discovery Project [DP110101188], National Key R&D Program of China (2016YFA0200200), DICP & QIBEBT (Grant DICP & QIBEBT UN201702), Dalian National Laboratory For Clean Energy (DNL), CAS. Authors also acknowledge the use of Deakin Advanced Characterization Facilities. All authors discussed the results and contributed equally.

Keywords: additive free electrode • hybrid Nb₂O₅-TiO₂• safe anode • sputtering technique • lithium-ion batteries

- [1] Y. Tang, Y. Zhang, W. Li, B. Ma, X. Chen, *Chem. Soc. Rev.* **2015**, *44*, 5926.
- [2] V. Etacheri, R. Marom, R. Elazari, G. Salitra, D. Aurbach, *Energy Environ. Sci.* **2011**, *4*, 3243.
- [3] G. E. Blomgren, *J. Electrochem. Soc.* **2017**, *164*, A5019.
- [4] Z. Chen, I. Belharouak, Y. K. Sun, K. Amine, *Adv. Funct. Mater.* **2013**, *23*, 959.
- [5] H. Ren, R. B. Yu, J. Y. Wang, Q. Jin, M. Yang, D. Mao, D. Kisailus, H. J. Zhao, D. Wang, *Nano Lett.* **2014**, *14*, 6679.
- [6] Y. Luo, J. Luo, J. Jiang, W. Zhou, H. Yang, X. Qi, H. Zhang, H. J. Fan, D. Y. W. Yu, C. M. Li, T. Yu, *Energy Environ. Sci.* **2012**, *5*, 6559.
- [7] Z. Wang, L. Zhou, X. W. Lou, *Adv. Mater.* **2012**, *24*, 1903.
- [8] Z. Yang, D. Choi, S. Kerisit, K. M. Rosso, D. Wang, J. Zhang, G. Graff, J. Liu, *J. Power Sources* **2009**, *192*, 588.
- [9] Y. Zhang, Y. Tang, W. Li, X. Chen, *ChemNanoMat* **2016**, *2*, 764.
- [10] E. Baudrin, S. Cassaignon, M. Koelsch, J. P. Jolivet, L. Dupont, J. M. Tarascon, *Electrochem. Commun.* **2007**, *9*, 337.
- [11] P. Kubiak, M. Pfanzenla, J. Geserick, U. Hörmann, N. Hüsing, U. Kaiser, M. Wohlfahrt-Mehrens, *J. Power Sources* **2009**, *194*, 1099.
- [12] Y. Liu, L. Lin, W. Zhang, M. Wei, *Scientific Reports* **2017**, *7*, 7204.
- [13] V. Augustyn, J. Come, M.A. Lowe, J.W. Kim, P.L. Taberna, S.H. Tolbert, H.D. Abruña, P. Simon, B. Dunn, *Nat. Mater.* **2013**, *12*, 518.
- [14] J. Come, V. Augustyn, J.W. Kim, P. Rozier, P.L. Taberna, P. Gogotsi, J.W. Long, B. Dunn, P. Simon, *J. Electrochem. Soc.* **2014**, *161*, A718.
- [15] J.W. Kim, V. Augustyn, B. Dunn, *Adv. Energy Mater.* **2012**, *2*, 141.
- [16] M. M. Rahman, R. A. Rani, A. Z. Sadek, A. S. Zoofakar, M. R. Field, T. Ramireddy, K. K. Zadeh, Y. Chen, *J. Mater. Chem. A* **2013**, *1*, 11019.
- [17] K. Brezesinski, J. Wang, J. Haetge, C. Reitz, S. O. Steinmueller, S. H. Tolbert, B. M. Smarsly, B. Dunn, T. Brezesinski, *J. Am. Chem. Soc.* **2010**, *132*, 6982.
- [18] X. Wang, G. Li, Z. Chen, V. Augustyn, X. Ma, G. Wang, B. Dunn, Y. Lu, *Adv. Energy Mater.* **2011**, *1*, 1089.
- [19] G. Li, X. Wang, X. Ma, *J. Energy Chem.* **2013**, *22*, 357.
- [20] M. Wei, K. Wei, M. Ichihara, H. Zhou, *Electrochem. Commun.* **2008**, *10*, 980.
- [21] H. Shim, Y. H. Jin, S. D. Seo, S. H. Lee, D. W. Kim, *ACS Nano* **2011**, *5*, 443.
- [22] P. G. Bruce, B. Scrosati, J. M. Tarascon, *Angew. Chem. Int. Ed.* **2008**, *47*, 2930.
- [23] Y. G. Wang, H. Q. Li, P. He, E. Hosono, H. S. Zhou, *Nanoscale* **2010**, *2*, 1294.
- [24] Z. Chen, V. Augustyn, J. Wen, Y. W. Zhang, M. Q. Shen, B. Dunn, Y. F. Lu, *Adv. Mater.* **2011**, *23*, 791.
- [25] I. Kovalenko, D. G. Bucknall, G. Yushin, *Adv. Funct. Mater.* **2010**, *20*, 3979.
- [26] M.H. Park, K. Kim, J. Kim, J. Cho, *Adv. Mater.* **2010**, *22*, 415.
- [27] J. Gao, M.A. Lowe, H.C.D. Abruña, *Chem. Mater.* **2011**, *23*, 3223.
- [28] Z.S. Wu, W. Ren, L. Wen, L. Gao, J. Zhao, Z. Chen, G. Zhou, F. Li, H.M. Cheng, *ACS Nano* **2010**, *4*, 3187.
- [29] H. Wang, L.F. Cui, Y. Yang, C. H. Sanchez, J.T. Robinson, Y. Liang, Y. Cui, H. Dai, *J. Am. Chem. Soc.* **2010**, *132*, 13978.
- [30] L. Sun, W. Liu, Y. Cui, Y. Zhang, H. Wang, S. Liu, B. Shan, *Green Chem.* **2018**, DOI: 10.1039/c8gc01683f.
- [31] D. H. Ha, M. A. Islam, R. D. Robinson, *Nano Lett.* **2012**, *12*, 5122.
- [32] S. Grugeon, S. Laruelle, R. Herrera-Urbina, L. Dupont, P. Poizot, J.M. Tarascon, *J. Electrochem. Soc.* **2001**, *148*, A285.
- [33] C.K. Chan, H.L. Peng, G. Liu, K. McIlwrath, X.F. Zhang, R.A. Huggins, Y. Cui, *Nat. Nanotechnol.* **2008**, *3*, 31.
- [34] A.M. Chockla, J.T. Harris, V.A. Akhavan, T.D. Bogart, V.C. Holmberg, C. Steinhagen, C.B. Mullins, K.J. Stevenson, B.A. Korgel, *J. Am. Chem. Soc.* **2011**, *133*, 20914.
- [35] Y. Li, X. Lv, J. Li, *Appl. Phys. Lett.* **2009**, *95*, 113102.
- [36] C.C. Li, Q.H. Li, L.B. Chen, T.H. Wang, *J. Mater. Chem.* **2011**, *21*, 11867.
- [37] H. Wu, G. Chan, J.W. Choi, I. Ryu, Y. Yao, M.T. McDowell, S.W. Lee, A. Jackson, Y. Yang, L. Hu, Y. Cui, *Nat. Nanotechnol.* **2012**, *7*, 310.
- [38] X. Yu, L. Xin, Y. Liu, W. Zhao, B. Li, X. Zhou, H. Shena, *RSC Adv.* **2016**, *6*, 27094.
- [39] W. Shi, X. Rui, J. Zhu, Q. Yan, *J. Phys. Chem. C* **2012**, *116*, 26685.
- [40] M. Srivastava, J. Singh, T. Kuila, R. K. Layek, N. H. Kime, J.H. Lee, *Nanoscale* **2015**, *7*, 4820.
- [41] J. Wang, Q. Deng, M. Li, K. Jiang, J. Zhang, Z. Hu, J. Chu, *Scientific Reports* **2017**, *7*, 8903.
- [42] S. Ge, H. Jia, H. Zhao, Z. Zheng, L. Zhang, *J. Mater. Chem.* **2010**, *20*, 3052.
- [43] Y.Y. Zhao, S.P. Pang, C.J. Zhang, Q.X. Zhang, L. Gu, X.H. Zhou, G.C. Li, G. L. Cui, *J. Solid State Electrochem.* **2013**, *17*, 1479.
- [44] Z.N. Wan, R. Cai, S.M. Jiang, Z.P. Shao, *J. Mater. Chem.* **2012**, *22*, 17773.
- [45] J.S. Chen, X. W. Lou, *J. Power Sources* **2010**, *195*, 2905.
- [46] X. Y. Yu, H. B. Wu, L. Yu, F. X. Ma, X. W. (David) Lou, *Angew. Chem. Int. Ed.* **2015**, *54*, 4001.
- [47] J. Li, Z. Tang, Z. Zhang, *Electrochem. Commun.* **2005**, *7*, 894.
- [48] M.M. Rahman, J.Z. Wang, M. F. Hassan, S. L. Chou, D. Wexler, H. K. Liu, *J. Power Sources* **2010**, *195*, 4297.
- [49] J. Wang, Y. Zhou, Y. Hu, R. O'Hayre, Z. Shao, *J. Phys. Chem. C* **2011**, *115*, 2529.
- [50] J. Li, Z. Tang, Z. Zhang, *Electrochem Solid-State Lett.* **2005**, *8*, A316.
- [51] M.M. Rahman, J. Z. Wang, D. Wexler, Y. Y. Zhang, X. J. Li, S. L. Chou, H. K. Liu, *J. Solid State Electrochem.* **2010**, *14*, 571.
- [52] G. Kim, C. Jo, W. Kim, J. Chun, S. Yoon, J. Lee, W. Choi, *Energy Environ. Sci.* **2013**, *6*, 2932.
- [53] M. Liu, C. Yan, Y. Zhang, *Scientific Reports* **2015**, *5*, 8326.
- [54] S. Liu, J. Zhou, Z. Cai, G. Fang, A. Pan, S. Liang, *Nanotechnology* **2016**, *27*, 46LT01.
- [55] M. Sasidharan, N. Gunawardhana, M. Yoshio, K. Nakashima, *Mater. Res. Bull.* **2012**, *47*, 2161.
- [56] T. Lan, H. Qiu, F. Xie, J. Yang, M. Wei, *Scientific Reports* **2015**, *5*, 8498.
- [57] M. Zhen, X. Guo, G. Gao, Z. Zhou, L. Liu, *Chem. Commun.* **2014**, *50*, 11915.
- [58] D. McNulty, E. Carroll, C. O'Dwyer, *Adv. Energy Mater.* **2017**, *7*, 1602291.
- [59] F. Zhang, L. Qi, *Adv. Sci.* **2016**, *3*, 1600049.

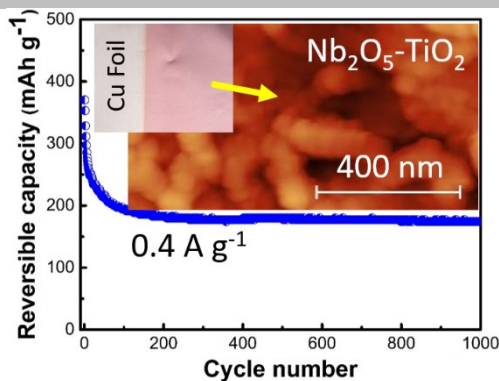
ARTICLE

Entry for the Table of Contents (Please choose one layout)

Layout 1:

ARTICLE

A radio frequency sputtering technique is developed to fabricate high performance lithium-ion battery anode of Nb₂O₅-TiO₂ without incorporation of any reagents in the process.



Md Mokhlesur Rahman,^{*,[a]} Mengqi Zhou,^[a] Irin Sultana,^[a] Srikanth Mateti,^[a] Alexey Falin,^[a] Lu Hua Li,^[a] Zhong-Shuai Wu,^[b] and Ying Chen^{*,[a]}

Page No. – Page No.

Additive-free hybrid anode of Nb₂O₅-TiO₂ towards low-cost and safe lithium-ion batteries: a green electrode material produced by an environmentally friendly process

Layout 2:

ARTICLE

((Insert TOC Graphic here))

Author(s), Corresponding Author(s)*

Page No. – Page No.

Title

Text for Table of Contents